Fast hadron freeze-out generator. II. Noncentral collisions

N. S. Amelin[*] and R. Lednicky[†]
Joint Institute for Nuclear Research, Dubna, Moscow Region, RU-141980, Russia

I. P. Lokhtin, L. V. Malinina,[‡] and A. M. Snigirev
M. V. Lomonosov Moscow State University, D. V. Skobeltsyn Institute of Nuclear Physics, RU-119991, Moscow, Russia

Iu. A. Karpenko and Yu. M. Sinyukov
Bogoliubov Institute for Theoretical Physics, Kiev, 03143, Ukraine

I. Arsene[§] and L. Bravina
Department of Physics, University of Oslo, Norway
(Received 7 November 2007; published 17 January 2008)

The fast Monte Carlo procedure of hadron generation developed in our previous work is extended to describe noncentral collisions of nuclei. We consider different possibilities to introduce appropriate asymmetry of the freeze-out hypersurface and flow velocity profile. For comparison with other models and experimental data, we demonstrate the results based on the standard parametrizations of the hadron freeze-out hypersurface and flow velocity profile assuming either a common chemical and thermal freeze-out or the chemically frozen evolution from chemical to thermal freeze-out. The C++ generator code is written under the ROOT framework and is available for public use at http://uhkm.jinr.ru/.

DOI: 10.1103/PhysRevC.77.014903 PACS number(s): 25.75.Dw, 24.10.Lx, 25.75.Gz

I. INTRODUCTION

In the preceding work [1], we developed a Monte Carlo (MC) simulation procedure, and the corresponding C++ code allowing for a fast but realistic description of multiple hadron production in central relativistic heavy ion collisions. A high generation speed and easy control through input parameters make our MC generator code particularly useful for detector studies. The generator code is quite flexible and allows the user to add other scenarios and freeze-out surface parametrizations as well as additional hadron species in a simple manner. We have compared the BNL Relativistic Heavy Ion Collider (RHIC) experimental data on central Au+Au collisions with our MC generation results obtained within the single freeze-out scenario with Bjorken-like and Hubble-like freeze-out surface parametrizations. Although simplified, such a scenario nevertheless allowed a reasonable description of particle spectra and femtoscopic momentum correlations to be obtained. This description can be further improved by introducing finite emission duration and extending the table of the included resonances; the single freeze-out scenario is, however, less successful in describing the data on elliptic flow (see Sec. III).

The particle densities at the chemical freeze-out stage are too high (see, e.g., Ref. [2]) to consider particles as free streaming and to associate this stage with the thermal freeze-out one. In this work, we have implemented as an option a more sophisticated scenario of thermal freeze-out: the system expands, hydrodynamically with frozen chemical composition, cools down, and finally decays at some thermal freeze-out hypersurface. The RHIC experimental data are compared with our MC generation results obtained within this thermal freeze-out scenario. We do not consider here a more complex freeze-out scenario taking into account continuous particle emission (see, e.g., Ref. [3]).

In the present paper, we also extend the fast Monte Carlo procedure of hadron generation developed in our previous work [1] to describe noncentral collisions of nuclei. One of the most spectacular features of the RHIC data is large elliptic flow [4]. The development of a strong flow is well described by the hydrodynamic models and requires short time scale and large pressure gradients, attributed to strongly interacting systems. However, results of hydrodynamic models significantly disagree with the data on femtoscopic momentum correlations (compare Ref. [5] with, e.g., Ref. [6]), related with the space-time characteristics of the system at freeze-out. Usually, the hadronic cascade models underestimate the momentum anisotropy and overestimate the source sizes (e.g., Refs. [7–9]). Some sophisticated hybrid models (e.g., a multiphase transport (AMPT) model [10]) reproduce the elliptic flow and the correlation radii but with different sets of model parameters.

Successful attempts to describe simultaneously the momentum-space measurements and the freeze-out coordinate-space data were done in several models which make experimental data fitting within some parametrizations of freeze-out hypersurface: the Kiev-Nantes model [3], blast-wave parametrizations [11–13], and the Buda-Lund

[*]Deceased.
[†]Also at Institute of Physics AS CR, 18221 Praha 8, Czech Republic.
[‡]Also at Joint Institute for Nuclear Research, Dubna, Moscow Region, 141980, Russia.
[§]Also at Institute for Space Sciences, Bucharest-Magurele, Romania.

hydrodynamic approach [14]. All these approaches use the hydrodynamically inspired parametrizations of freeze-out hypersurface and help in understanding the full freeze-out scenario at RHIC.

In this article, we analyze the RHIC data at $\sqrt{s_{NN}} = 200$ GeV and try to use the same set of model parameters for the description of both the momentum-space observables, i.e., transverse mass m_t spectra and p_t dependence of elliptic flow, and the freeze-out coordinate-space observables, i.e., k_t dependence and azimuthal angle Φ dependence of the correlation radii. The chemical composition of the fireball was fixed in our previous article [1] by the particle ratios analysis.

The paper is organized as follows. Section II is devoted to the description of the main modifications of the model [1] needed to take into consideration noncentral collisions. In Sec. III, the example calculations are compared with the RHIC experimental data. We summarize and conclude in Sec. IV.

II. FREEZE-OUT SURFACE PARAMETRIZATIONS

The extension of our MC generator to noncentral collisions demands mainly the modification of freeze-out hypersurface parametrizations (Sec. V of Ref. [1]) and does not practically influence the generation procedure itself (Sec. VI of Ref. [1]). Therefore, we focus on these modifications only in considering the popular Bjorken-like and Hubble-like freeze-out parametrizations used, respectively, in the so-called blast wave [11] and Cracow [15] models as the example options in our MC generator. Similar parametrizations have been used in the hadron generator THERMINATOR [12]. As usual, in the Bjorken-like parametrization, we substitute the Cartesian coordinates t, z by the Bjorken ones [16]

$$\tau = (t^2 - z^2)^{1/2}, \quad \eta = \frac{1}{2}\ln\frac{t+z}{t-z}, \tag{1}$$

and introduce the the radial vector $\vec{r} \equiv \{x, y\} = \{r\cos\phi, r\sin\phi\}$, i.e.,

$$\begin{aligned} x^\mu &= \{\tau\cosh\eta, \vec{r}, \tau\sinh\eta\} \\ &= \{\tau\cosh\eta, r\cos\phi, r\sin\phi, \tau\sinh\eta\}. \end{aligned} \tag{2}$$

For a freeze-out hypersurface represented by the equation $\tau = \tau(\eta, r, \phi)$, the hypersurface element in terms of the coordinates η, r, ϕ becomes

$$d^3\sigma_\mu = \epsilon_{\mu\alpha\beta\gamma}\frac{dx^\alpha\, dx^\beta\, dx^\gamma}{d\eta\, dr\, d\phi}\, d\eta\, dr\, d\phi, \tag{3}$$

where $\epsilon_{\mu\alpha\beta\gamma}$ is the completely antisymmetric Levy-Civita tensor in four dimensions with $\epsilon^{0123} = -\epsilon_{0123} = 1$. Generally, the freeze-out hypersurface is represented by a set of equations $\tau = \tau_j(\eta, r, \phi)$, and Eq. (3) should be substituted by the sum of the corresponding hypersurface elements. For the simplest and frequently used freeze-out hypersurface $\tau = \text{const}$, one has

$$\begin{aligned} d^3\sigma_\mu &= n_\mu\, d^3\sigma = \tau d^2\vec{r}\, d\eta\{\cosh\eta, 0, 0, -\sinh\eta\}, \\ d^3\sigma &= \tau\, d^2\vec{r}\, d\eta, \quad n^\mu = \{\cosh\eta, 0, 0, \sinh\eta\}. \end{aligned} \tag{4}$$

In noncentral collisions, the shape of the emission region in the transverse x–y plane can be approximated by an ellipse (as usual, the z–x plane coincides with the reaction plane). The ellipse radii $R_x(b)$ and $R_y(b)$ at a given impact parameter b are usually parametrized [11,17–19] in terms of the spatial anisotropy $\epsilon(b) = (R_y^2 - R_x^2)/(R_x^2 + R_y^2)$ and the scale factor $R_s(b) = [(R_x^2 + R_y^2)/2]^{1/2}$, that is,

$$R_x(b) = R_s(b)\sqrt{1-\epsilon(b)}, \quad R_y(b) = R_s(b)\sqrt{1+\epsilon(b)}. \tag{5}$$

Then from the ellipse equation,

$$\frac{x^2}{R_x^2} + \frac{y^2}{R_y^2} = 1, \tag{6}$$

follows the explicit dependence of the fireball transverse radius $R(b, \phi)$ on the azimuthal angle ϕ:

$$R(b,\phi) = R_s(b)\frac{\sqrt{1-\epsilon^2(b)}}{\sqrt{1+\epsilon(b)\cos 2\phi}}; \tag{7}$$

particularly, $R(b, 0) = R_x(b)$ and $R(b, \pi/2) = R_y(b)$. To reduce the number of free parameters, we assume here a simple scaling option [20]

$$R_s(b) = R_s(b=0)\sqrt{1-\epsilon_s(b)}, \tag{8}$$

where $R_s(b = 0) \equiv R$ is the fireball freeze-out transverse radius in central collisions. It means that the dimensionless ratio $R_s(b)/R_s(0)$ at the freeze-out moment depends on the collision energy, the radius R_A of the colliding (identical) nuclei, and the impact parameter b through a dimensionless $\epsilon_s(b)$ only. It should be noted that both $\epsilon_s(b)$ and the fireball freeze-out eccentricity $\epsilon(b)$ are determined by the eccentricity $\epsilon_0(b) = b/(2R_A)$ of the elliptical overlap of the colliding nuclei at the initial moment, when

$$\left.\frac{R_s(b)}{R_s(b=0)}\right|_{\epsilon(b)=\epsilon_0(b)} \equiv \frac{R_s(b)_{\text{initial}}}{R_A} = \sqrt{1-\epsilon_0(b)}. \tag{9}$$

Since $\epsilon_s(0) = \epsilon(0) = \epsilon_0(0) = 0$, one can assume that $\epsilon_s(b) \simeq \epsilon(b)$ at sufficiently small values of the impact parameter b. It appears that the use of the simple ansatz $\epsilon_s(b) = \epsilon(b)$ allows one to achieve the absolute normalization of particle spectra correct within ~10% up to $b \simeq R_A$ (see Sec. III C).

If the system evolution were driven by the pressure gradients, the expansion would be stronger in the direction of the short ellipse x axis (in the reaction plane), where the pressure gradient is larger than in the direction of the long ellipse y axis (see, e.g., Ref. [6]). The typical hydrodynamic evolution scenario is shown in Fig. 1. During the evolution, the initial system coordinate anisotropy $\epsilon_0(b)$ is transformed into the momentum anisotropy $\delta(b)$. According to the hydrodynamic calculations, the spatial eccentricity almost disappears and the momentum anisotropy saturates at rather early evolution stage before freeze-out. As we do not trace the evolution here, we will consider the spatial and momentum anisotropies $\epsilon(b)$ and $\delta(b)$ as free parameters.

For central collisions, the fluid flow four-velocity $u^\mu(t, \vec{x}) = \gamma(t, \vec{x})\{1, \vec{v}(t, \vec{x})\} \equiv \gamma(t, \vec{x})\{1, \vec{v}_\perp(t, \vec{x}), v_z(t, \vec{x})\}$ at a point $\vec{x}$ and time t was parametrized [1] in terms of the

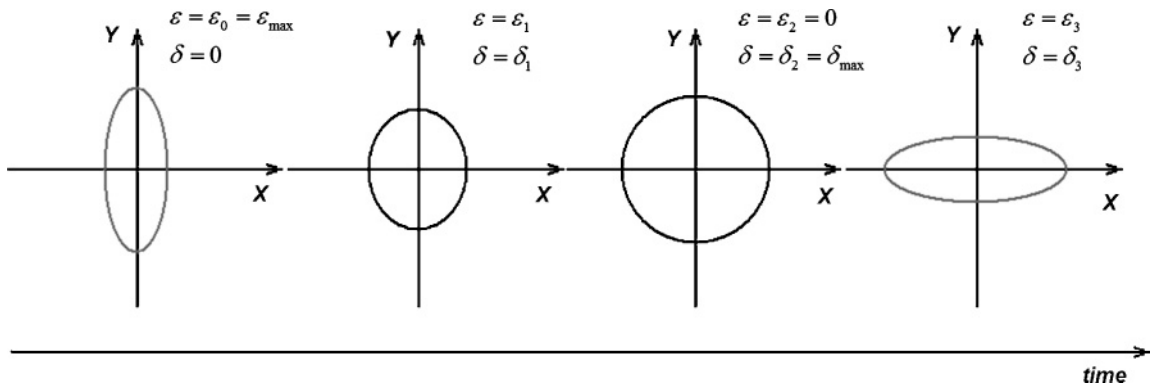

FIG. 1. Typical hydrodynamic evolution scenario.

longitudinal (z) and transverse ($\perp$) fluid flow rapidities

$$\eta_u(t,\vec{x}) = \frac{1}{2}\ln\frac{1+v_z(t,\vec{x})}{1-v_z(t,\vec{x})},$$
$$\rho_u(t,\vec{x}) = \frac{1}{2}\ln\frac{1+v_\perp(t,\vec{x})\cosh\eta_u(t,\vec{x})}{1-v_\perp(t,\vec{x})\cosh\eta_u(t,\vec{x})}, \tag{10}$$

where $v_\perp = |\vec{v}_\perp|$ is the magnitude of the transverse component of the flow three-velocity $\vec{v} = \{v_\perp\cos\phi_u, v_\perp\sin\phi_u, v_z\}$, i.e.,

$$\begin{aligned} u^\mu(t,\vec{x}) &= \{\cosh\rho_u\cosh\eta_u, \sinh\rho_u\cos\phi_u, \sinh\rho_u\sin\phi_u, \\ &\quad \cosh\rho_u\sinh\eta_u\} \\ &= \{(1+u_\perp^2)^{1/2}\cosh\eta_u, \vec{u}_\perp, (1+u_\perp^2)^{1/2}\sinh\eta_u\}, \end{aligned} \tag{11}$$

$\vec{u}_\perp = \gamma\vec{v}_\perp = \gamma_\perp\cosh\eta_u\vec{v}_\perp$, and $\gamma_\perp = \cosh\rho_u$. However, unlike the transverse isotropic parametrization ($\phi_u = \phi$), now the azimuthal angle ϕ_u of the fluid velocity vector is not necessarily identical to the spatial azimuthal angle ϕ, because of the nonzero flow anisotropy parameter $\delta(b)$ [18,19], that is,

$$\begin{aligned} u^\mu(t,\vec{x}) &= \{\gamma_\phi\cosh\tilde{\rho}_u\cosh\eta_u, \sqrt{1+\delta(b)}\sinh\tilde{\rho}_u\cos\phi, \\ &\quad \sqrt{1-\delta(b)}\sinh\tilde{\rho}_u\sin\phi, \gamma_\phi\cosh\tilde{\rho}_u\sinh\eta_u\}, \end{aligned} \tag{12}$$

where

$$\gamma_\phi = \sqrt{1+\delta(b)\tanh^2\tilde{\rho}_u\cos 2\phi}, \tag{13}$$

$$\tan\phi_u = \sqrt{\frac{1-\delta(b)}{1+\delta(b)}}\tan\phi. \tag{14}$$

The transverse flow rapidity ρ_u is related to $\tilde{\rho}_u$ by

$$u_\perp = \sinh\rho_u = \sqrt{1+\delta(b)\cos 2\phi}\sinh\tilde{\rho}_u. \tag{15}$$

Note, that for $\delta(b) = 0$ (i.e., $\phi_u = \phi$), Eq. (12) reduces to Eq. (11) which was applied in Refs. [20,21]. In Ref. [19], $\delta(b)$ is obtained by fitting the model prediction to the measured elliptic flow coefficient v_2.

Further, we assume the longitudinal boost invariance [16] $\eta_u = \eta$, which is a good approximation for the highest RHIC energies at the midrapidity region. To account for the violation of the boost invariance, we have also included in the code an option corresponding to the substitution of the uniform distribution of the space-time longitudinal rapidity η in the interval $[-\eta_{\max}, \eta_{\max}]$ by a Gaussian distribution $\exp(-\eta^2/2\Delta\eta^2)$ with a width parameter $\Delta\eta = \eta_{\max}$. The presence of the "oscillation term" $\sqrt{1+\delta(b)\cos 2\phi}$ in the transverse component $u_\perp$ of the flow velocity in Eq. (15) allows us to use the simple linear profile for $\tilde{\rho}_u$ without introducing additional parameters for each centrality (b) unlike other models, namely,

$$\tilde{\rho}_u = \frac{r}{R_s(b)}\rho_u^{\max}(b=0), \tag{16}$$

where $\rho_u^{\max}(b=0)$ is the maximal transverse flow rapidity for central collisions. At such normalization and $\delta(b) > \epsilon(b)$, the maximal transverse flow $(u_\perp, \rho_u)$ is achieved at $\phi = 0$, i.e., along the x axis as it should be according to the hydrodynamic scenario described above (Fig. 1). (Although $\tilde{\rho}_u$ has a maximum at $\phi = \pi/2$!).

Here one should note that the "popular parametrization" of transverse flow rapidity used in Ref. [11] (and implemented as an option in our MC generator also), i.e.,

$$\rho_u = \tilde{r}[\rho_0(b) + \rho_2(b)\cos 2\phi_u], \tag{17}$$

where

$$\tilde{r} \equiv \sqrt{\left(\frac{r\cos\phi}{R_x}\right)^2 + \left(\frac{r\sin\phi}{R_y}\right)^2} = \frac{r}{R(b,\phi)}, \tag{18}$$

is the "normalized elliptical radius," in which $\rho_0(b)$ and $\rho_2(b)$ are the two fitting parameters, is close to our parametrization, and gives similar results for the observables under consideration. In the parametrization of Ref. [11], the boost is perpendicular to the elliptical subshell on which the source element is found: $\tan\phi_u = (R_x^2/R_y^2)\tan\phi = (1-\epsilon)/(1+\epsilon)\tan\phi$ and $\delta(b) = 2\epsilon(b)/(1+\epsilon^2(b))$. It is interesting to note that for sufficiently weak transverse flows, $\rho_u \leqslant 1$, considered here, one can put $\sinh\rho_u \simeq \rho_u$ and obtain our parametrization from that of Ref. [11] by the substitutions

$$\frac{\rho_0(b)}{R(b,\phi)} \to \frac{\rho_u^{\max}(b=0)}{R_s(b)},$$
$$1 + \frac{\rho_2(b)}{\rho_0(b)}\cos 2\phi_u \to \sqrt{1+\delta(b)\cos 2\phi}. \tag{19}$$

Thus, in the case of moderate transverse flows, one can obtain the same result either by fixing the direction of the flow

velocity vector but allowing for the azimuthal dependence of the flow rapidity or by allowing for arbitrary direction of the flow velocity vector but assuming azimuthally independent flow rapidity.

At $\tau = \text{const}$, the total effective volume for particle production in the case of noncentral collisions becomes

$$V_{\text{eff}} = \int_{\sigma(t,\vec{x})} d^3\sigma_\mu(t,\vec{x}) u^\mu(t,\vec{x}) = \tau \int_0^{2\pi} d\phi \int_0^{R(b,\phi)} (n_\mu u^\mu) r\, dr \int_{\eta_{\min}}^{\eta_{\max}} d\eta, \quad (20)$$

where $(n_\mu u^\mu) = \cosh\tilde{\rho}_u \sqrt{1+\delta(b)\tanh^2\tilde{\rho}_u \cos 2\phi}$.

We also consider the Cracow model scenario [15] corresponding to the Hubble-like freeze-out hypersurface $\tau_H = (t^2 - x^2 - y^2 - z^2)^{1/2} = \text{const}$. Introducing the longitudinal space-time rapidity η according to Eq. (1) and the transverse space-time rapidity $\rho = \sinh^{-1}(r/\tau_H)$, one has [22]

$$x^\mu = \tau_H \{\cosh\eta\cosh\rho, \sinh\rho\cos\phi, \times \sinh\rho\sin\phi, \sinh\eta\cosh\rho\}, \quad (21)$$

$\tau_H = \tau_B/\cosh\rho$. Representing the freeze-out hypersurface by the equation $\tau_H = \tau_H(\eta,\rho,\phi) = \text{const}$, one finds from Eq. (3):

$$d^3\sigma = \tau_H^3 \sinh\rho\cosh\rho\, d\eta\, d\rho\, d\phi = \tau_H\, d\eta d^2\vec{r}, \quad n^\mu(t,\vec{x}) = x^\mu(t,\vec{x})/\tau_H. \quad (22)$$

With the additional flow anisotropy parameter $\delta(b)$, the flow four-velocity is parametrized as [19]

$$u^\mu(t,\vec{x}) = \left\{\gamma_\phi^H \cosh\rho\cosh\eta, \sqrt{1+\delta(b)}\sinh\rho\cos\phi, \times\sqrt{1-\delta(b)}\sinh\rho\sin\phi, \gamma_\phi^H\cosh\rho\sinh\eta\right\}, \quad (23)$$

where

$$\gamma_\phi^H = \sqrt{1+\delta(b)\tanh^2\rho\cos 2\phi}. \quad (24)$$

The effective volume corresponding to $r = \tau_H\sinh\rho < R(b,\phi)$ and $\eta_{\min} \leqslant \eta \leqslant \eta_{\max}$ is

$$V_{\text{eff}} = \int_{\sigma(t,\vec{x})} d^3\sigma_\mu(t,\vec{x}) u^\mu(t,\vec{x}) = \tau_H \int_0^{2\pi} d\phi \int_0^{R(b,\phi)} (n_\mu u^\mu) r\, dr \int_{\eta_{\min}}^{\eta_{\max}} d\eta, \quad (25)$$

with

$$(n_\mu u^\mu) = \cosh^2\rho\left[\sqrt{1+\delta(b)\tanh^2\rho\cos 2\phi} - \tanh^2\rho\left(\sqrt{1+\delta(b)}\cos^2\phi + \sqrt{1-\delta(b)}\sin^2\phi\right)\right] \simeq 1 + o(\delta^2(b)). \quad (26)$$

Our MC procedure for generating the freeze-out hadron multiplicities, four-momenta, and four-coordinates for central collisions has been described in detail in Ref. [1]. For noncentral collisions, only the generation of the transverse radius r is slightly different, taking place in the azimuthally dependent interval $[0, R(b,\phi)]$.

III. INPUT PARAMETERS AND EXAMPLE CALCULATIONS

A. Model input parameters

First, we summarize the input parameters which control the execution of our MC hadron generator in the case of Bjorken-like and Hubble-like parametrizations and should be specified for different energies, ion beams, and event centralities.

(i) Thermodynamic parameters at chemical freeze-out: temperature T^{ch} and chemical potentials per unit charge $\widetilde{\mu}_B, \widetilde{\mu}_S, \widetilde{\mu}_Q$. As an option, an additional parameter $\gamma_s \leqslant 1$ takes into account the strangeness suppression according to the partially equilibrated distribution [23,24]

$$f_i(p^{*0}; T, \mu_i, \gamma_s) = \frac{g_i}{\gamma_s^{-n_i^s}\exp\left([p^{*0} - \mu_i]/T\right) \pm 1}, \quad (27)$$

where n_i^s is the number of strange quarks and antiquarks in a hadron i, p^{*0} is the hadron energy in the fluid element rest frame, and $g_i = 2J_i + 1$ is the spin degeneracy factor Optionally, the parameter γ_s can be fixed using its phenomenological dependence on the temperature and baryon chemical potential [25].

(ii) Volume parameters: the fireball transverse radius $R(b=0)$ [determined in central collisions; in noncentral collisions, we use the scaling option (8,9), to recalculate $R(b)$ from $R(b=0)$], the freeze-out proper time τ, and its standard deviation $\Delta\tau$ (emission duration) [26].

(iii) Maximal transverse flow rapidity $\rho_u^{\max}(b=0)$ for Bjorken-like parametrization in central collisions.

(iv) Maximal space-time longitudinal rapidity $\eta_{\max}$ which determines the rapidity interval $[-\eta_{\max}, \eta_{\max}]$ in the collision center-of-mass system. To account for the violation of the boost invariance, we have included in the code an option corresponding to the substitution of the uniform distribution of the space-time longitudinal rapidity η in the interval $[-\eta_{\max}, \eta_{\max}]$ by a Gaussian distribution $\exp(-\eta^2/2\Delta\eta^2)$ with a width parameter $\Delta\eta = \eta_{\max}$ (see, e.g., Refs. [20,27]).

(v) Impact parameter range: minimal $b_{\min}$ and maximal $b_{\max}$ impact parameters.

(vi) Flow anisotropy parameter $\delta(b)$ in Bjorken-like and Hubble-like parametrizations [or $\rho_0(b)$ and $\rho_2(b)$ in the blast-wave parametrization of Ref. [11]].

(vii) Coordinate anisotropy parameter $\epsilon(b)$.

(viii) Thermal freeze-out temperature T^{th} (if single freeze-out is considered, $T^{\text{th}} = T^{\text{ch}}$).

(ix) Effective chemical potential of π^+ at thermal freeze-out $\mu_\pi^{\text{eff,th}}$ (0, if single freeze-out is considered).

(x) Parameter which enables/disables weak decays.

The parameters used to simulate central collisions are given in Table I. The parameters determined in central collisions for $T^{\text{th}} = 0.1$ GeV with $\tau = 8.0$ fm/c, $R(b=0) = 10$ fm, $\Delta\tau = 2.0$ fm/c, and $\rho_u^{\max}(b=0) = 1.1$ (fourth column in Table I) were used to simulate Au+Au collisions at $\sqrt{s_{NN}} = 200$ GeV

TABLE I. Model parameters for central Au+Au collisions at $\sqrt{s_{NN}} = 200$ GeV for different thermal freeze-out temperatures $T^{\rm th}$ (GeV). Chemical freeze-out parameters are $T^{\rm ch} = 0.165$ GeV, $\widetilde{\mu}_B = 0.028$ GeV, $\widetilde{\mu}_S = 0.007$ GeV, and $\widetilde{\mu}_Q = -0.001$ GeV.

Parameter	$T^{\rm th} = 0.165$	$T^{\rm th} = 0.130$	$T^{\rm th} = 0.100$
τ, fm/c	7.0	7.2	8.0
$\Delta\tau$, fm/c	2.0	2.0	2.0
$R(b=0)$, fm	9.0	9.5	10.0
$\rho_u^{\max}(b=0)$	0.65	0.9	1.1
$\mu_\pi^{\rm eff,\,th}$	0	0.10	0.11

at different centralities. The additional parameters needed only for noncentral collisions are given in Table II.

B. Different chemical and thermal freeze-outs

Since the assumption of a common chemical and thermal freeze-out can hardly be justified (see, e.g., Ref. [2]), we consider here a more complicated scenario with different chemical and thermal freeze-outs.

The mean particle numbers $\bar{N}_i^{\rm th}$ at thermal freeze-out can be determined using the following procedure [2]. In our preceding article [1], we fixed the temperature and chemical potentials at chemical freeze-out by fitting the ratios of the numbers of (quasi)stable particles. The common factor $V_{\rm eff}^{\rm ch}$ and thus the absolute particle and resonance numbers was fixed by pion multiplicities. Within the concept of chemically frozen evolution, these numbers are assumed to be conserved except for corrections due to decay of some part of the short-lived resonances that can be estimated from the assumed chemical to thermal freeze-out evolution time. Then one can calculate the mean numbers of different particles and resonances reaching a (common) thermal freeze-out hypersurface. At a given thermal freeze-out temperature $T^{\rm th}$ these mean numbers can be expressed through the thermal effective volume $V_{\rm eff}^{\rm th}$ and the chemical potentials for each particle species $\mu_i^{\rm th}$. The latter can no longer be expressed in the form $\mu_i = \vec{q}_i\vec{\widetilde{\mu}}$, which is valid only for chemically equilibrated systems. For a given parametrization of the thermal freeze-out hypersurface, the thermal effective volume $V_{\rm eff}^{\rm th}$ (and thus all $\mu_i^{\rm th}$) can be fixed with the help of pion interferometry data.

In practical calculations, the particle number density $\rho_i^{\rm eq}(T,\mu_i)$ is represented in the form of a fast converging series [1], that is,

$$\rho_i^{\rm eq}(T,\mu_i) = \frac{g_i}{2\pi^2} m_i^2 T \sum_{k=1}^{\infty} \frac{(\mp)^{k+1}}{k} \exp\left(\frac{k\mu_i}{T}\right) K_2\left(\frac{km_i}{T}\right), \tag{28}$$

where K_2 is the modified Bessel function of the second order, and m_i and $g_i = 2J_i + 1$ are the mass and the spin degeneracy factor of particle i, respectively.

Using Eq. (28) and the assumption of the conservation of the particle number ratios from the chemical to thermal freeze-out evolution time, we obtain the following ratios for the i-particle specie to π^+:

$$\frac{\rho_i^{\rm eq}(T^{\rm ch},\mu_i)}{\rho_\pi^{\rm eq}(T^{\rm ch},\mu_i^{\rm ch})} = \frac{\rho_i^{\rm eq}(T^{\rm th},\mu_i^{\rm th})}{\rho_\pi^{\rm eq}(T^{\rm th},\mu_\pi^{\rm eff,\,th})}. \tag{29}$$

The absolute values of particles densities $\rho_i^{\rm eq}(T^{\rm th},\mu_i^{\rm th})$ are determined by the choice of the free parameter of the model: effective pion chemical potential $\mu_\pi^{\rm eff,\,th}$ at the temperature of thermal freeze-out $T^{\rm th}$. Assuming for the other particles (heavier then pions) the Boltzmann approximation in Eq. (28), one deduces from Eqs. (28) and (29) the chemical potentials of particles and resonances at thermal freeze-out:

$$\mu_i^{\rm th} = T^{\rm th} \ln\left(\frac{\rho_i^{\rm eq}(T^{\rm ch},\mu_i^{\rm ch})}{\rho_i^{\rm eq}(T^{\rm th},\mu_i=0)} \frac{\rho_\pi^{\rm eq}(T^{\rm th},\mu_\pi^{\rm eff,\,th})}{\rho_\pi^{\rm eq}(T^{\rm ch},\mu_i^{\rm ch})}\right). \tag{30}$$

The correct way to determine the best set of model parameters would be to fit all the observables together, as suggested in Ref. [27]; but for our MC-type model, this is technically impossible. For the example calculations with our model at RHIC energies, we choose $T^{\rm ch} = 0.165$ GeV and the thermal temperatures as in the analytical models which performed the successful fitting of RHIC data: $T^{\rm th} = T^{\rm ch} = 0.165$ GeV (Cracow model [15]) and $T^{\rm th} = 0.100$ GeV (blast-wave model [11]), and some arbitrary intermediate temperature $T^{\rm th} = 0.130$ GeV. It is well known (see, e.g., Ref. [2]) that the pion transverse spectra at thermal freeze-out can be described in two regimes: low temperature and large transverse flow on the one hand, and higher temperature and nonrelativistic transverse flow on the other hand (see Sec. III C). The low temperature regime seems to be preferable, because the strong transverse flow is expected to describe better the large inverse slopes of transverse spectra of the heavy hadrons (especially protons) and small correlation radii obtained at RHIC [3,11]. We present the calculated correlation radii in Sec. III E.

In the last version of FASTMC considered here, the new table of resonances was included. It contains 360 resonances and stable particles, instead of the 85 included in the previous versions. This particle table is produced from the SHARE [28] particle table excluding any not well established resonances states. The decays of resonances are controlled by the decay lifetime $1/\Gamma$, where Γ is the resonance width specified in the particle table, and the decays occur with the probability

TABLE II. Model parameters for Au+Au collisions at $\sqrt{s_{NN}} = 200$ GeV at different centralities (c). Chemical freeze-out parameters are $T^{\rm ch} = 0.165$ GeV, $\widetilde{\mu}_B = 0.028$ GeV, $\widetilde{\mu}_S = 0.007$ GeV, and $\widetilde{\mu}_Q = -0.001$ GeV. Thermal freeze-out parameters are $T^{\rm th} = 0.1$ GeV, $\mu_\pi^{\rm eff,\,th} = 0.11$ GeV. Volume parameters determined in the central collisions are $R(b=0) = 10.0$ fm, $\tau = 8.0$ fm/c, $\rho_u^{\max}(b=0) = 1.1$.

Parameter	$c =$ 0–5%	$c =$ 5–10%	$c =$ 10–20%	$c =$ 20–30%	$c =$ 30–40%	$c =$ 40–60%
$b_{\min}/R_A$	0	0.447	0.632	0.894	1.095	1.265
$b_{\max}/R_A$	0.447	0.632	0.894	1.095	1.265	1.549
$\epsilon(b)$	0	0	0	0.1	0.15	0.15
$\delta(b)$	0.05	0.08	0.12	0.25	0.34	0.36

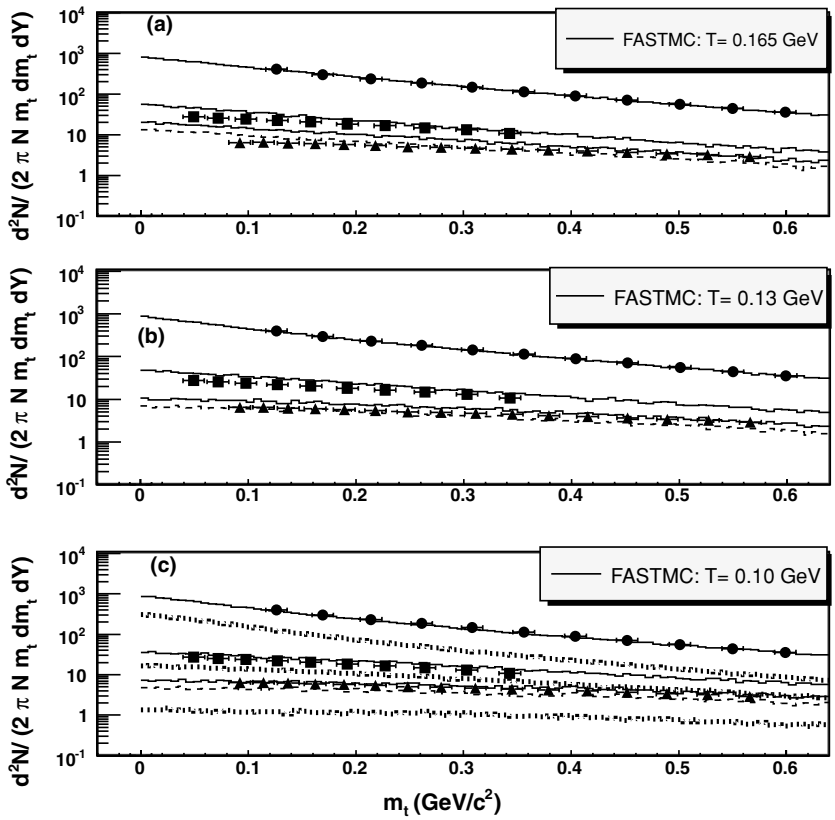

FIG. 2. m_t spectra (in c^4/GeV^2) measured by the STAR Collaboration [29] for π^+ (circles), K^+ (squares), and p (up-triangles)at 0–5% centrality in comparison with model calculations at $T^{\mathrm{th}} = 0.165$ (a), 0.130 (b), 0.100 (c) GeV, with the parameters from Table I, for protons with weak decays taken into account (solid lines); for protons with weak decays not taken into account (dashed lines). The direct π^+, K^+, and p contributions are shown on (c) by dotted lines.

density $\Gamma \exp(-\Gamma\tau)$ in the resonance rest frame. Then the decay products are boosted to the reference frame in which the freeze-out hypersurface was defined. Because we need to compare our calculations with data from different experiments, we made it possible to switch on/off different decays based on their lifetimes (i.e., turn on/off weak decays). Only the two- and three-body decays are considered in our model. The branching ratios are also taken from the particle decay table produced from the SHARE decay table [28]. The cascade decays are also possible.

C. m_t spectra

In Fig. 2, the m_t spectra measured by the STAR Collaboration [29] at 0–5% centrality are shown for π^+, K^+, and p in comparison with the model calculations under the assumption of the common chemical and thermal freeze-out at $T^{\mathrm{th}} = T^{\mathrm{ch}} = 0.165$ GeV [Fig. 2(a)] and under the assumption that the thermal freeze-out at $T^{\mathrm{th}} = 0.100$, 0.130 GeV occurs after the chemical one [Figs. 2(b) and 2(c)].

The correction on weak decays was introduced by the STAR Collaboration in pion spectra only [29]. It was approximately 12% and was estimated from the measured K^0_s and Λ decays. In Ref. [29], the STAR Collaboration does not introduce the weak decay correction in proton spectra. To reproduce the STAR weak decay correction procedure, we excluded pions from K^0_s and Λ decays from pions m_t spectra in Fig. 2. The contribution of weak decays in the simulated proton spectra can be estimated from Fig. 2 by comparison of the solid lines (protons from K^0_s and Λ decays are included) and the dashed lines (without contribution of protons from the weak decays). The model parameters at different temperatures are presented in Table I. The parameters were optimized this way to obtain a good description of the pion m_t spectra and the correlation radii. The best description of the m_t spectra was achieved at $T^{\mathrm{th}} = 0.100$ GeV [Fig. 2(c)].

The same set of parameters T, $\rho_u^{\max}$, R, and τ which was determined for central collisions (Table I) was used for noncentral ones. The additional parameters of the model for noncentral collisions were coordinate and momentum asymmetries: ϵ and δ (Table II). At the freeze-out moment, we consider them as free parameters because we do not trace the evolution here. The influence of the choice of ϵ and δ on m_t spectra averaged over azimuthal angle φ is negligible. The decrease of the effective volume in noncentral collisions [Eq. (20)] due to nonzero values of ϵ and δ allows us to obtain the correct absolute normalization of m_t spectra without introduction of the additional parameters. In Fig. 3, the m_t spectra measured by the STAR Collaboration [29] are shown for π^+, K^+ and p at centralities: 0–5%, 5–10%, 10–20%, 20–30%, 30–40%, and 40–50% in comparison with the model calculations which assume that the thermal freeze-out at $T^{\mathrm{th}} = 0.1$ GeV occurs after the chemical one (solid lines). It appears that the procedure described in Sec. II allows one to achieve the absolute normalization of pion spectra correct within ~13%.

D. Elliptic flow

Following a standard procedure [30,31], we make a Fourier expansion of the hadron distribution in the azimuthal angle φ

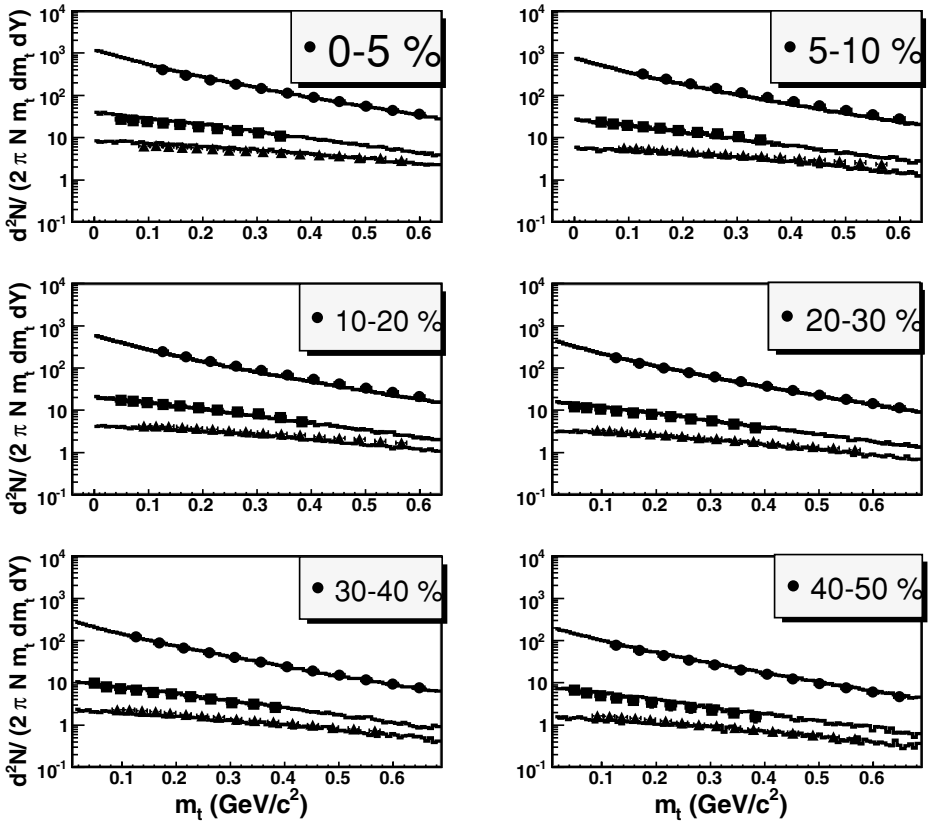

FIG. 3. m_t spectra (in c^4/GeV^2) measured by the STAR Collaboration [29] for π^+ (circles), K^+ (squares), and p (up-triangles) at different centralities compared with our FASTMC calculations at $T^{\mathrm{th}} = 0.100\,\mathrm{GeV}$ (solid lines) with the parameters from Tables I and II.

at mid-rapidity:

$$\frac{dN}{d^2 p_t\, dy} = \frac{dN}{2\pi p_t\ dp_t\, dy}(1 + 2v_2 \cos 2\varphi + 2v_4 \cos 4\varphi + \cdots). \quad (31)$$

The elliptic flow coefficient v_2 is defined as the second-order Fourier coefficient,

$$v_2 = \frac{\int_0^{2\pi} d\varphi \cos 2(\varphi - \psi_R) \frac{d^3N}{dy\, d\varphi p_t\, dp_t}}{\int_0^{2\pi} d\varphi \frac{d^3N}{dy\, d\varphi\ p_t\, dp_t}}, \quad (32)$$

where ψ_R is the reaction plane angle (in our generation, $\psi_R = 0$), and y and p_t are, respectively, the rapidity and transverse momentum of the particle under consideration.

The value of v_2 is an important signature of the physics occurring in heavy ion collisions. According to the typical hydrodynamic scenario shown in Fig. 1, the elliptic flow is generated mainly during the high density phase of the fireball evolution. The system driven by the internal pressure gradients expands more strongly in its short direction (into the direction of the impact parameter x in Fig. 1, which is chosen as a "positive" direction) than in the perpendicular one ("negative" direction, y in Fig. 1) where the pressure gradients are smaller. Figure 1 illustrates qualitatively that the initial spacial anisotropy of the system disappears during the evolution, while the momentum anisotropy grows. The developing of strong flow observed at RHIC requires a short time scale and large pressure gradients, which are characteristics of a strongly interacting system. The reason for the generation of v_2 at the early times is that the system should be hot and dense; when the system cools and become less dense, the development of large pressure gradients becomes impossible. The elliptic flow coefficient v_2 depends on the transverse momentum p_t, the impact parameter b or centrality, as well as, the type of the considered particle. All these dependencies have been measured at RHIC [32].

The p_t dependence of v_2 measured by the STAR Collaboration [32] for charged particles at centralities 0–5%, 5–10%, 10–20%, 20–30%, 30–40%, and 40–60% is shown in Fig. 4 in comparison with our MC calculations obtained with the optimal model parameters from Table II. The calculations were performed under the assumption that thermal freeze-out at $T^{\mathrm{th}} = 0.1$ GeV occurs after the chemical one at $T^{\mathrm{th}} = 0.165$ GeV.

The calculations under the assumption of the common chemical and thermal freeze-out at $T^{\mathrm{th}} = T^{\mathrm{ch}} = 0.165$ GeV do not demonstrate good agreement with the experimental data at small $p_t < 0.4$ GeV/c for centralities larger than 20%; irrespective of the choice of ϵ and δ, one cannot get a satisfactory description in the whole p_t range (see e.g., Fig. 5).

E. Correlation radii

The parameters of the model presented in Table I were optimized to obtain the best description of the pion m_t spectra and the correlation radii in the following cases: under the assumption of the common chemical and thermal freeze-out at $T^{\mathrm{th}} = T^{\mathrm{ch}} = 0.165$ GeV and under the assumption that the thermal freeze-out at $T^{\mathrm{th}} = 0.100, 0.130$ GeV occurs after the chemical one. In Fig. 6, the fitted correlation radii R_{out}, R_{side},

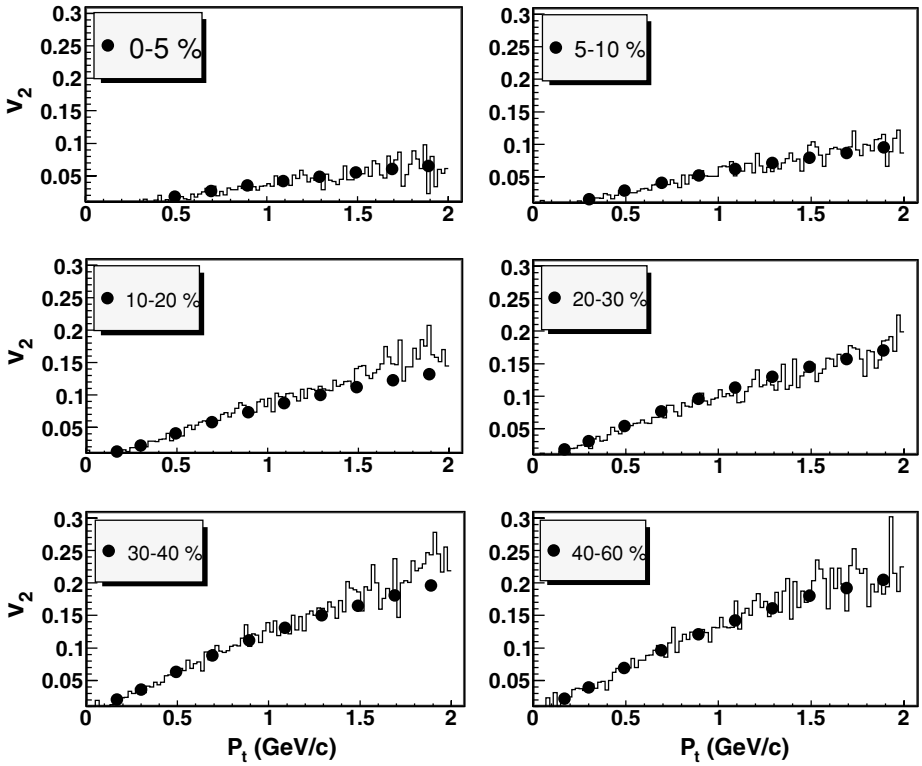

FIG. 4. p_t dependence of v_2 measured by the STAR Collaboration [32] (points) for charged particles at different centralities in comparison with our FASTMC calculations (solid lines) at $T^{\rm th} = 0.100$ GeV with the parameters from Tables I and II.

and $R_{\rm long}$ are compared with those measured by the STAR Collaboration [5]. The three-dimensional correlation function was fitted with the standard Gaussian formula:

$$\mathrm{CF}(p_1, p_2) = 1 + \lambda \exp\left(-R^2_{\rm out} q^2_{\rm out} - R^2_{\rm side} q^2_{\rm side} - R^2_{\rm long} q^2_{\rm long}\right), \qquad (33)$$

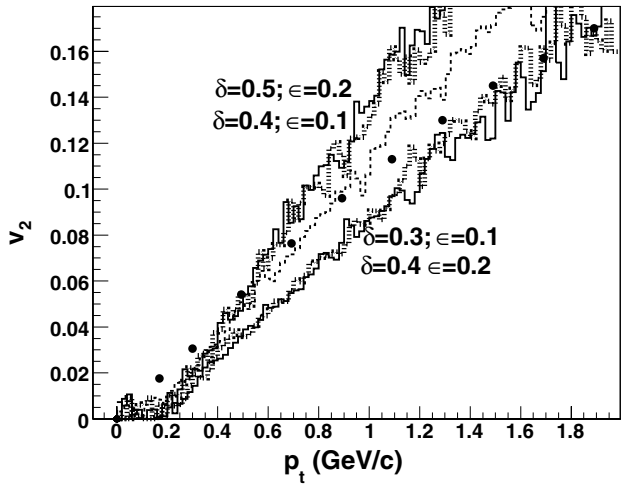

FIG. 5. p_t dependence of v_2 measured by the STAR Collaboration [32] (points) for charged particles at centrality 20–30% compared with our FASTMC calculations under assumption of the single freeze-out at $T^{\rm th} = T^{\rm ch} = 0.165$ GeV. The different sets of coordinate and momentum asymmetry parameters were tried: $\epsilon = 0.1, \delta = 0.3$ (lower solid line), $\epsilon = 0.2, \delta = 0.4$ (lower dotted line), $\epsilon = 0.1, \delta = 0.4$ (upper solid line), $\epsilon = 0.2, \delta = 0.5$ (upper dotted line), $\epsilon = 0.15, \delta = 0.4$ (dashed line).

where $\vec{q} = \vec{p}_1 - \vec{p}_2 = (q_{\rm out}, q_{\rm side}, q_{\rm long})$ is the relative three-momentum of two identical particles with four-momenta p_1 and p_2. The form of Eq. (33) assumes azimuthal symmetry of the production process [33]. Generally, e.g., in the case of the correlation analysis with respect to the reaction plane, all three cross terms $q_i q_j$ can be significant [27]. We will consider this case below. We choose the longitudinal comoving system (LCMS) as the reference frame [34]. In the LCMS, each pair is emitted transverse to the reaction axis so that the pair rapidity vanishes. The parameter λ measures the correlation strength.

The regime with the large temperature $T^{\rm th} = T^{\rm ch} = 0.165$ GeV was tested in Ref. [1]. We repeated this test here with the new resonances table and the additional parameter $\Delta\tau$ [Fig. 6(a), dashed line]. We have found that these modifications lead to a better description of the correlation radii. In Fig. 6(a), bottom panel (dashed line), the intercept λ is larger than the experimental one, but taking into account the secondary pions from the weak decays essentially improves the description of the λ [Fig. 6(a), bottom, solid line].

In Figs. 6(b) and 6(c), we consider the lower thermal freeze-out temperatures: 0.130, 0.100 GeV. The secondary pions coming from the weak decays were taken into account.

It is worth to note a good description of the correlation radii (within ~10% accuracy) altogether with the absolute value of the m_t spectra in the scenario with a low temperature thermal freeze-out of chemically frozen hadron-resonance gas. There are three important reasons for this success. First, a relatively small (compared with dynamic models) effective volume of the system $\sim\tau R^2$ that reduces the correlation radii. Second, relatively large transverse flow in the model that further

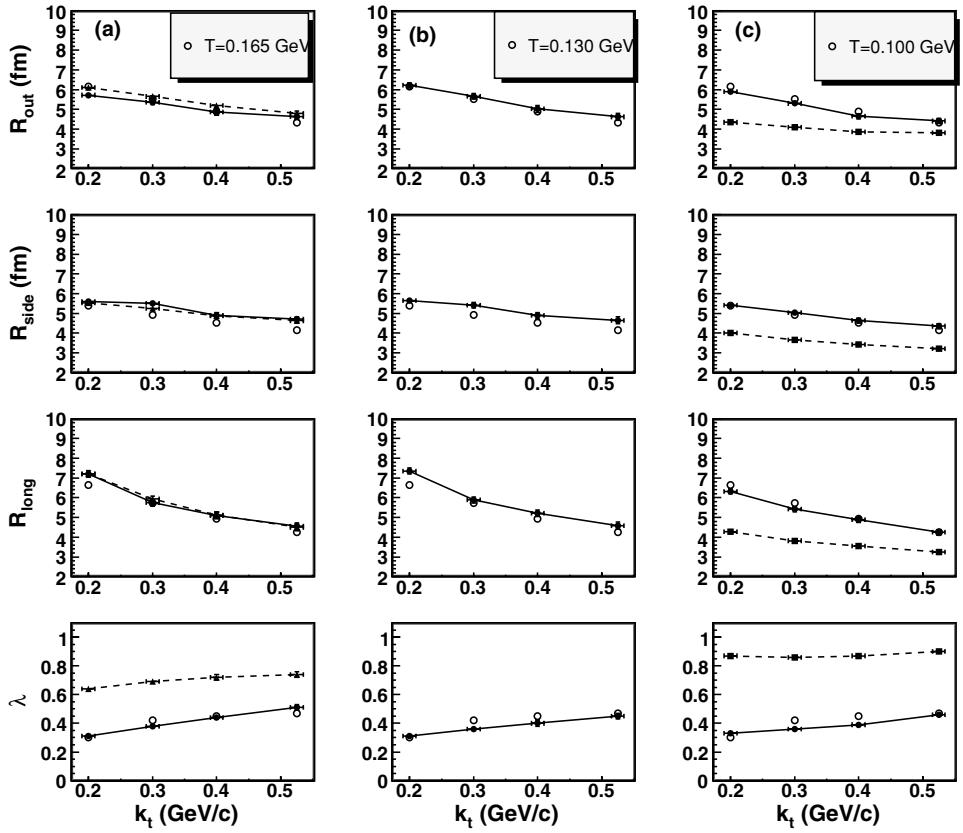

FIG. 6. π^+ correlation radii at midrapidity in central Au+Au collisions at $\sqrt{s_{NN}} = 200$ GeV from the STAR experiment [5] (open circles) and MC calculations within the Bjorken-like model with the parameters presented in Table I in different intervals of the pair transverse momentum k_t. The full calculation with resonances (a), (b). (a) Single freeze-out $T^{\rm ch} = T^{\rm th} = 0.165$ GeV, no weak decays (dashed line), with weak decays (solid line); (b) thermal freeze-out at $T^{\rm th} = 0.130$ GeV occurs after the chemical one, weak decays are taken into account (solid line); (c) the full calculation with resonances, weak decays are taken into account at $T^{\rm th} = 0.100$ GeV (solid line), the direct pions only (dotted lines).

reduces the radii. Third, a rather large effective pion chemical potential which is needed to describe the absolute value of the pion spectra at relatively small effective volumes; it reduces correlation radii at small p_t and so makes their m_t behavior flatter. This reduction happens because the homogeneity length of the Bose-Einstein distribution for low-p_t pions vanishes when the pion chemical potential approaches the pion mass (see also Ref. [35] for the analysis of the reduction of the pion correlation radii near the point of the Bose-Einstein condensation in static systems). We do not consider here the question of whether such conditions could be realized in realistic dynamical models.

It should be noted that the description of the k_t dependence of the correlation radii has been achieved within $\sim$10% accuracy for all three considered thermal temperatures: $T^{\rm th} = 0.165, 0.130, 0.100$ GeV. However, at lower temperatures there is more flexibility in the simultaneous description of particle spectra and correlations because the effective volume is not strictly fixed as it is in the case of the single freeeze-out ($T^{\rm th} = T^{\rm ch} = 0.165$ GeV). In the present work, we have not attempted to fit the model parameters ($T^{\rm th}$, R, τ, $\mu_\pi^{\rm eff,\,th}$) since it is a rather complicated task requiring a lot of computer time. We have performed only example calculations with several sets of the parameters.

In noncentral collisions, the measurement of azimuthally sensitive correlation radii provides additional information about the source shape. For the corresponding femtoscopic formalism with respect to the reaction plane, see, e.g., Refs. [18,27]. In the absence of azimuthal symmetry, the three additional cross terms contribute to the Gaussian parametrization of the correlation function in Eq. (33):

$$\mathrm{CF}(p_1, p_2) = 1 + \lambda \exp\big(- R_{\rm o}^2 q_{\rm out}^2 - R_{\rm s}^2 q_{\rm side}^2 - R_{\rm l}^2 q_{\rm long}^2 - 2R_{\rm os}^2 q_{\rm out} q_{\rm side} - 2R_{\rm ol}^2 q_{\rm out} q_{\rm long} - 2R_{\rm sl}^2 q_{\rm side} q_{\rm long}\big). \tag{34}$$

In the boost-invariant case, the transverse-longitudinal cross terms $R_{\rm ol}^2$ and $R_{\rm sl}^2$ vanish in the LCMS frame, while the important outside $R_{\rm os}^2$ cross term is present.

In the Gaussian approximation, the radii in Eq. (34) are related to space-time variances via the set of equations [18,27]

$$\begin{aligned} R_{\rm s}^2 &= 1/2(\langle\tilde{x}^2\rangle + \langle\tilde{y}^2\rangle) - 1/2(\langle\tilde{x}^2\rangle - \langle\tilde{y}^2\rangle)\cos(2\Phi) - \langle\tilde{x}\tilde{y}\rangle \sin(2\Phi), \\ R_{\rm o}^2 &= 1/2(\langle\tilde{x}^2\rangle + \langle\tilde{y}^2\rangle) + 1/2(\langle\tilde{x}^2\rangle - \langle\tilde{y}^2\rangle)\cos(2\Phi) + \langle\tilde{x}\tilde{y}\rangle \sin(2\Phi)) \\ &\quad - 2\beta_\perp(\langle\tilde{t}\tilde{x}\rangle \cos(\Phi) + \langle\tilde{t}\tilde{y}\rangle \sin(\Phi)) + \beta_\perp^2\langle\tilde{t}^2\rangle, \\ R_{\rm l}^2 &= \langle\tilde{z}^2\rangle - 2\beta_l\langle\tilde{t}\tilde{z}\rangle + \beta_l^2\langle\tilde{t}^2\rangle, \\ R_{\rm s}^2 &= \langle\tilde{x}\tilde{y}\rangle \cos(2\Phi) - 1/2(\langle\tilde{x}^2\rangle - \langle\tilde{y}^2\rangle)\sin(2\Phi) + \beta_\perp(\langle\tilde{t}\tilde{x}\rangle \sin(\Phi) - \langle\tilde{t}\tilde{y}\rangle \cos(\Phi)), \end{aligned} \tag{35}$$

where $\beta_l = k_z/k^0$, $\beta_\perp = k_\perp/k^0$, and $\Phi = \angle(\vec{k}_\perp, \vec{b})$ is the azimuthal angle of the pair three-momentum $\vec{k}$ with respect to the reaction plane z-x determined by the longitudinal direction and the direction of the impact parameter vector $\vec{b} = (x, 0, 0)$; the space-time coordinates $\tilde{x}^\mu$ are defined relative to the

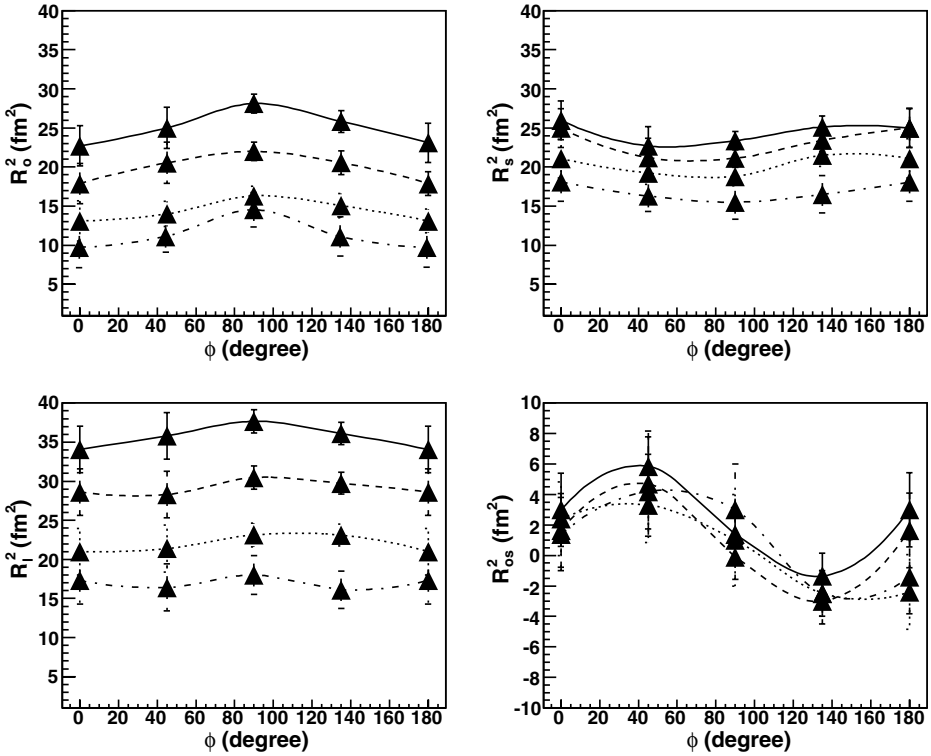

FIG. 7. Simulated with FASTMC squared correlation radii vs the azimuthal angle Φ of the $\pi^+\pi^+$ pair with respect to the reaction plane, 20–30% centrality events in k_T (GeV/c) intervals: $0.15 < k_T < 0.25$ (solid line), $0.25 < k_T < 0.35$ (dashed line), $0.35 < k_T < 0.45$ (dotted line), $0.45 < k_T < 0.60$ (dotted-dashed line). Simulation was done with the special set of parameters: $T^{\rm th} = 0.1$ GeV, $\rho_u^{\rm max}(b = 0) = 1.0$; $R(b = 0) = 11.5$ fm, $\tau = 7.5$ fm/c, $\Delta\tau = 0$ fm/c, $\epsilon = 0.1$ and $\delta = 0.25$; weak decays were not taken into account.

effective source center $\langle x^\mu \rangle$: $\widetilde{x}^\mu = x^\mu - \langle x^\mu \rangle$. The averages are taken with the source emission function $S(t, \vec{x}, k)$ [18]

$$\langle f(t, \vec{x}) \rangle = \frac{\int d^4x f(t, \vec{x}) S(t, \vec{x}, k)}{\int d^4x S(t, \vec{x}, k)}. \tag{36}$$

The illustrative calculations of the correlation radii as a function of the azimuthal angle Φ were done with the following fast MC parameters: $T^{\rm th} = 0.1$ GeV, $\rho_u^{\rm max}(b = 0) = 1.0$; $R(b = 0) = 11.5$ fm, $\tau = 7.5$ fm/c, $\Delta\tau = 0.$ fm/c, $\epsilon = 0.1$, and $\delta = 0.25$. The azimuthal dependence of the correlation radii in different k_t intervals is shown in Fig. 7.

The R_s^2 oscillates downward, in the same phase as the RHIC source extended out of plane [36], which means the larger sideward radius viewed from the x direction (in the reaction plane) than from the y direction (out of plane). The source has small coordinate asymmetry $\epsilon = 0.1$, and it is almost round (as in Fig. 1 step 3); however, the emission zone, or "homogeneity region," varies with Φ because of the nonisotropic flow.

IV. CONCLUSIONS

We have developed a MC simulation procedure, and the corresponding C++ code, that allows a fast realistic description of multiple hadron production both in central and noncentral relativistic heavy ion collisions. A high generation speed and an easy control through input parameters make our MC generator code particularly useful for detector studies. As options, we have implemented two freeze-out scenarios with coinciding and with different chemical and thermal freeze-outs. We have compared the RHIC experimental data with our MC generation results obtained within the single and separated freeze-out scenarios with Bjorken-like freeze-out surface parametrization.

Fixing the temperatures of the chemical and thermal freeze-outs at 0.165 and 0.100 GeV, respectively, and using the same set of model parameters as for the central collisions, we have described single-particle spectra at different centralities with the absolute normalization correct within ∼13%.

The comparison of the RHIC v_2 measurements with our MC generation results shows that the scenario with two separated freeze-outs is more favorable for the description of the p_t dependence of the elliptic flow.

The description of the k_t dependence of the correlation radii has been achieved within ∼10% accuracy. The experimentally observed values of the correlation strength parameter λ has been reproduced because the weak decays were accounted for.

The analysis of the azimuthal dependence of the correlation radii indicates that the source considered in the model oscillates downward, in the same phase as RHIC source extended out of plane.

The understanding achieved of the reasons leading to a good simultaneous description of particle spectra, elliptic flow, and femtoscopic correlations within the considered simple model could be useful for building the complete dynamic picture of the matter evolution in $A+A$ collisions.

ACKNOWLEDGMENTS

We thank A. Kisiel, W. Broniowski, and W. Florkowski for permission to use the particle data table from SHARE used in their THERMINATOR code. We also thank Eu. Zabrodin, B. V. Batyunia, and L. I. Sarycheva for useful discussions. The research has been carried out within the scope of the

ERG (GDRE): Heavy ions at ultra-relativistic energies—a European Research Group comprising IN2P3/CNRS, Ecole des Mines de Nantes, Universite de Nantes, Warsaw University of Technology, JINR Dubna, ITEP Moscow, and Bogoliubov Institute for Theoretical Physics NAS of Ukraine. The investigations have been partially supported by the IRP AVOZ10480505, by the Grant Agency of the Czech Republic under Contract No. 202/07/0079, by Grant No. LC07048 of the Ministry of Education of the Czech Republic, by Grant No. UKP1-2613-KV-04 of the U.S. Civilian Research and Development Foundation (CRDF) and Fundamental Research State Fund of Ukraine, by Agreement No. F7/209-2004 and a grant from the Physics and Astronomics Division of NASU /017U000396 (19.12.06), Fundamental Research State Fund of Ukraine, by Agreement No. F25/718-2007 and a grant from DLR(Germany)-MESU (Ukraine) for UKR 06/008 Project, and by Grant No. N08-02-91001-CERN-a from the Russian Foundation for Basic Research.

[1] N. S. Amelin, R. Lednicky, T. A. Pocheptsov, I. P. Lokhtin, L. V. Malinina, A. M. Snigirev, Iu. A. Karpenko, and Yu. M. Sinyukov, Phys. Rev. C **74**, 064901 (2006).
[2] S. V. Akkelin, P. Braun-Munzinger, and Yu. M. Sinyukov, Nucl. Phys. **A710**, 439 (2002).
[3] M. S. Borysova, Yu. M. Sinyukov, S. V. Akkelin, B. Erazmus, and Iu. A. Karpenko, Phys. Rev. C **73**, 024903 (2006).
[4] C. Adler *et al*. (STAR Collaboration), Phys. Rev. Lett. **87**, 182301 (2001).
[5] J. Adams *et al*. (STAR Collaboration), Phys. Rev. C **71**, 044906 (2005).
[6] P. F. Kolb, J. Sollfrank, and U. W. Heinz, Phys. Lett. **B459**, 667 (1999).
[7] D. Hardtke and S. A. Voloshin, Phys. Rev. C **61**, 024905 (2000).
[8] R. J. M. Snellings, A. M. Poskanzer, and S. A. Voloshin, nucl-ex/9904003.
[9] M. Bleicher and H. Stoecker, Phys. Lett. **B526**, 309 (2002).
[10] Bin Zhang, C. M. Ko, Bao-An Li, and Ziwei Lin, Phys. Rev. C **61**, 067901 (2000); Zi-wei Lin, Subrata Pal, C. M. Ko, Bao-An Li, and Bin Zhang, *ibid*. **64**, 011902(R) (2001).
[11] F. Retiere and M. A. Lisa, Phys. Rev. C **70**, 044907 (2004).
[12] A. Kisiel, T. Taluc, W. Broniowski, and W. Florkowski, Comput. Phys. Commun. **174**, 669 (2006).
[13] W. Florkowski, W. Broniowski, A. Kisiel, and J. Pluta, Acta Phys. Pol. B **37**, 3381 (2006).
[14] M. Csanad, T. Csörgö, and B. Lörstad, Nucl. Phys. **A742**, 80 (2004).
[15] W. Florkowski and W. Broniowski, Acta. Phys. Pol. B **35**, 2895 (2004).
[16] J. D. Bjorken, Phys. Rev. D **27**, 140 (1983).
[17] P. Huovinen, P. F. Kolb, U. Heinz, P. V. Ruuskanen, and S. A. Voloshin, Phys. Lett. **B503**, 58 (2001).
[18] U. A. Wiedemann, Phys. Rev. C **57**, 266 (1998).
[19] W. Broniowski, A. Baran, and W. Florkowski, AIP Conf. Proc. **660**, 185 (2003).
[20] I. P. Lokhtin and A. M. Snigirev, Eur. Phys. J. C **45**, 211 (2006).
[21] U. W. Heinz and S. M. H. Wong, Phys. Rev. C **66**, 014907 (2002).
[22] T. Csörgö and B. Lörstad, Phys. Rev. C **54**, 1390 (1996).
[23] G. D. Yen, M. I. Gorenstein, W. Greiner, and S. N. Yang, Phys. Rev. C **56**, 2210 (1997).
[24] J. Rafelski, Phys. Lett. **B262**, 333 (1981).
[25] F. Becattini, J. Manninen, and M. Gazdzicki, Phys. Rev. C **73**, 044905 (2006).
[26] L. V. Bravina *et al*., Nucl. Phys. **A698**, 383 (2002).
[27] U. A. Wiedemann and U. Heinz, Phys. Rep. **319**, 145 (1999).
[28] G. Torrieri *et al*., Comput. Phys. Commun. **167**, 229 (2005).
[29] J. Adams *et al*. (STAR Collaboration), Phys. Rev. Lett. **92**, 112301 (2004).
[30] S. Voloshin and Y. Zang, Z. Phys. C **70**, 665 (1996).
[31] A. M. Poskanzer and S. A. Voloshin, Phys. Rev. C **58**, 1671 (1998).
[32] J. Adams *et al*. (STAR Collaboration), Phys. Rev. C **72**, 014904 (2005).
[33] M. I. Podgoretskii, Sov. J. Nucl. Phys. **37**, 272 (1983).
[34] T. Csörgö and S. Pratt, In Proceedings of the Workshop on Heavy Ion Physics, KFKI-1991-28/A, p. 75 (unpublished).
[35] R. Lednicky, V. Lyuboshitz, K. Mikhailov, Yu. Sinyukov, A. Stavinsky, and B. Erazmus, Phys. Rev. C **61**, 034901 (2000).
[36] J. Adams *et al*. (STAR Collaboration), Phys. Rev. Lett. **93**, 012301 (2004).